Mon. Not. R. Astron. Soc. **000**, 1–?? (2012) Printed 26 April 2013 (MN LaTeX style file v2.2)

arXiv:1304.6723v1 [astro-ph.CO] 24 Apr 2013

The SLUGGS survey: Probing the supermassive black hole connection with bulges and haloes using red and blue globular cluster systems

Vincenzo Pota[1], Alister W. Graham [1], Duncan A. Forbes[1], Aaron J. Romanowsky[2,3], Jean P. Brodie[3], Jay Strader[4]

[1] *Centre for Astrophysics & Supercomputing, Swinburne University, Hawthorn VIC 3122, Australia*
[2] *Department of Physics and Astronomy, San José State University, One Washington Square, San Jose, CA 95192, USA*
[3] *University of California Observatories, 1156 High Street, Santa Cruz, CA 95064, USA*
[4] *Department of Physics and Astronomy, Michigan State University, East Lansing, Michigan 48824, USA*
Email: vpota@astro.swin.edu.au, dforbes@astro.swin.edu.au

Released 2012 Xxxxx XX

ABSTRACT
Understanding whether the bulge or the halo provides the primary link to the growth of supermassive black holes has strong implications for galaxy evolution and supermassive black hole formation itself. In this paper, we approach this issue by investigating extragalactic globular cluster (GC) systems, which can be used to probe the physics of both the bulge and the halo of the host galaxy. We study the relation between the supermassive black hole masses $(M_{\rm BH})$ and the globular cluster system velocity dispersions $(\sigma_{\rm GC})$ using an updated and improved sample of 21 galaxies. We exploit the dichotomy of globular cluster system colours, to test if the blue and red globular clusters correlate differently with black hole mass. This may be expected if they trace the potentially different formation history of the halo and of the bulge of the host galaxy respectively. We find that $M_{\rm BH}$ correlates with the total GC system velocity dispersion, although not as strongly as claimed by recent work of Sadoun & Colin. We also examine the $M_{\rm BH} - \sigma_{\rm GC}$ relation for barred/bar-less and core/non-core galaxies, finding no significant difference, and for the first time we quantify the impact of radial gradients in the GC system velocity dispersion profile on the $M_{\rm BH} - \sigma_{\rm GC}$ relation. We additionally predict $M_{\rm BH}$ in 13 galaxies, including dwarf elliptical galaxies and the cD galaxy NGC 3311. We conclude that our current results cannot discriminate between the bulge/halo scenario. Although there is a hint that the red GC velocity dispersion might correlate better with $M_{\rm BH}$ than the blue GC velocity dispersion, the number statistics are still too low to be certain.

Key words: supermassive black holes - galaxies:star clusters – galaxies:evolution– galaxies: kinematics and dynamics

1 INTRODUCTION

Extragalactic globular clusters (GCs) may provide key insight into the connection between galaxies and supermassive black holes (SMBHs). GCs are typically old ($>$ 10 Gyr, Brodie & Strader 2006) and may have witnessed the events which formed the SMBH in the first place. Moreover, GC systems usually come in two subpopulations, thought to be the result of different formation mechanisms (e.g. Ashman & Zepf 1992; Forbes et al. 1997; Côté et al. 1998). The blue (metal-poor) subpopulation has been associated with galaxy halos (Forte et al. 2005; Moore et al. 2006; Forbes et al. 2012; Spitler et al. 2012). It may have originated in metal-poor dwarf galaxies at high redshift consequently accreted into the halo of larger systems (Elmegreen et al. 2012). The properties of the red (metal-rich) GCs are similar to those of the galaxy bulge (Strader et al. 2011; Forbes et al. 2012), perhaps because of a coeval formation, such as in a turbulent disk (Shapiro et al. 2010) or in a merger (Kruijssen et al. 2012). Therefore, if the growth of SMBHs is primarily driven by recent merger events, one might expect a stronger correlation between red GCs and SMBHs . Conversely, if the properties of SMBHs were set during the primordial formation of their host galaxies, we might expect a stronger correlation with blue GCs (Omukai et al. 2008; Mayer et al. 2010; Debattista et al. 2013).

There exists a surprisingly good correlation between the total number of GCs (both blue and red) per galaxy $(N_{\rm GC})$ and the black hole mass of galaxies $(M_{\rm BH})$. However, this does not necessarily imply a primary correlation between GCs and

© 2012 RAS

SMBHs (Jahnke & Macciò 2011). In fact, Snyder et al. (2011) argued this correlation to be indirect as expected if it was a consequence of the debated black hole fundamental plane (Hopkins et al. 2007; Graham 2008). Nevertheless, the $M_{\rm BH} - N_{\rm GC}$ relation has been shown to have an intriguingly small scatter at fixed $M_{\rm BH}$ (Burkert & Tremaine 2010; Harris & Harris 2011). Rhode (2012) has recently shown that these findings are driven by low number statistics, and that an improved galaxy sample returns a scatter at fixed $M_{\rm BH}$ which is larger than previously inferred. Rhode additionally found similar slopes and scatters for the relations for the blue and the red GCs.

Recently, Sadoun & Colin (2012) (hereafter SC12), have examined the correlation between the GC system velocity dispersion and $M_{\rm BH}$ for twelve galaxies, including the Milky Way. Their results suggest a tight correlation between $M_{\rm BH}$ and the velocity dispersion for both the red and blue GC subpopulations, with an intrinsic scatter ϵ always $\leqslant 0.33$ dex, indicating a very tight correlation. They also find that the red GCs are more closely correlated ($\epsilon = 0.22$ dex) with $M_{\rm BH}$ than the blue GCs ($\epsilon = 0.33$ dex).

In this paper we revisit the work of SC12 with an expanded sample of 21 galaxies and updated $M_{\rm BH}$ values. We supplemented our sample with high velocity resolution data from the ongoing SLUGGS survey (Pota et al. 2013) and we re-analysed literature data with the same method. We tested if the tight correlation seen for the red GCs is real or driven by sample selection or methodology biases. The outline of the paper is as follows. We describe the data in Section 2 and their analysis in Section 3. Results are then presented and discussed in Section 4. Conclusions are given in Section 5.

2 GALAXY SAMPLE

We study a subset of galaxies with direct $M_{\rm BH}$ measurements and with more than ten GC radial velocity measurements. From the literature, we compiled a list of 13 galaxies. This includes all the galaxies discussed in SC12, excluding the Milky Way, and two additional galaxies: NGC 253 (Olsen et al. 2004) and NGC 3585 (Puzia et al. 2004), not studied by SC12 because the uncertainties on the GC velocity dispersion were not quoted in the parent papers. The Milky Way is not included in this study because the results of Côté (1999) suggest that the still uncertain velocity dispersion of the Milky Way GC system is unusually large for its black hole mass. Moreover, the fact that the Milky Way GC analysis is carried out in three-dimensions rather than in projection, makes the comparison with other galaxies not straightforward. We also update the GC catalogue used by SC12 for NGC 4594 with the latest compilation of Alves-Brito et al. (2011). We note that SC12 used $M_{\rm BH}$ values from Gültekin et al. (2009) although more recent $M_{\rm BH}$ were sometimes available.

For NGC 224 (M31) we use the GC system velocity dispersion measurements from Lee et al. (2008), because their catalogue is not available on-line.

In regard to NGC 253, there are two public GC catalogues for this galaxy: Beasley & Sharples (2000) and Olsen et al. (2004), for a total 38 GCs. However, we were unable to find a reliable calibration offset between the radial velocities of the four GCs in common between these two datasets. We decided to use the Olsen catalogue only, because it is larger in size (24 GCs) than Beasley's dataset (14 GCs).

The biggest strength of our data set is the addition of a further 9 new early-type galaxies from the SLUGGS survey, one of which (NGC 4486) was already discussed in SC12. We use the most recent black hole mass measurements as summarized in McConnell & Ma (2012) and Graham & Scott (2012). This gives us a sample of 21 galaxies, nearly double the number used by SC12, which are listed in Table A1.

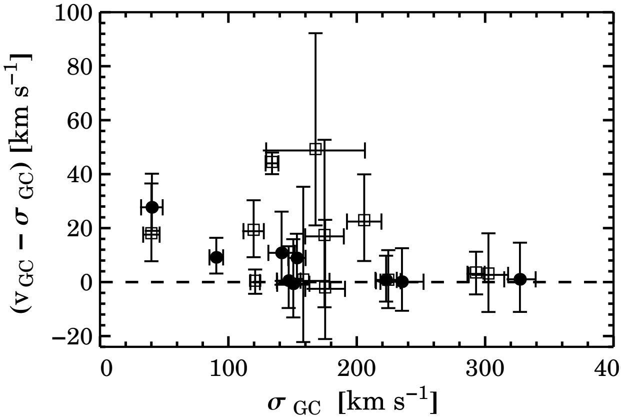

Figure 1. Difference between the rotation-subtracted velocity dispersion $\sigma_{\rm GC}$ and the rotation-included velocity dispersion $v_{\rm GC}$ without any colour split. Filled points and empty squares are the data from the SLUGGS survey and the literature respectively. The two quantities are generally consistent with each other, but they disagree by up to ~ 40 km s^{-1} in systems with significant rotation.

3 METHOD

3.1 The globular cluster system velocity dispersion

The stellar velocity dispersion, σ_*, used in the $M_{\rm BH} - \sigma_*$ relation is usually defined either as the luminosity-weighted velocity dispersion within $1/8^{\rm th}$ of an effective radius R_e, or within 1 R_e (σ_e), and/or as the central velocity dispersion (σ_0). Although they represent physically distinct quantities, σ_e and σ_0 have been reported to be consistent with each other (Gültekin et al. 2009). This stems from the fact that the velocity dispersion profiles vary only weakly within these regions (e.g., Emsellem et al. 2011).

The detection of extragalactic globular clusters occurs predominantly at $R \geqslant R_e$. Therefore none of the stellar velocity dispersion quantities are directly recovered with GC data. We define the GC system velocity dispersion in two different ways, which are similar to the quantities used for stellar data. This also takes into account that some GC systems can have a rotation component which is as large as that of the random motions (Beasley et al. 2006).

The first quantity, $\sigma_{\rm GC}$, assumes a Gaussian velocity distribution and it is defined as the standard deviation with respect to the model function (Côté et al. 2001):

$$v(\theta) = v_{\rm sys} + v_{\rm rot} \sin(\theta_0 - \theta), \quad (1)$$

which measures the GC rotation amplitude $v_{\rm rot}$ as a function of the azimuth θ, with θ_0 being the direction of the angular momentum vector and $v_{\rm sys}$ being the systemic velocity of the host galaxy. We use a variation on Equation 1, originally designed by Krajnović et al. (2006) for IFU data-cubes and then extended to sparsely sampled data by Proctor et al. (2009). We then minimise a χ^2 function (see Bergond et al. 2006) to compute the best fit parameters $(v_{\rm rot}, \sigma_{\rm GC}, \theta_0)$. Uncertainties were derived by bootstrapping the sample 1000 times to derive 68 per cent confidence intervals.

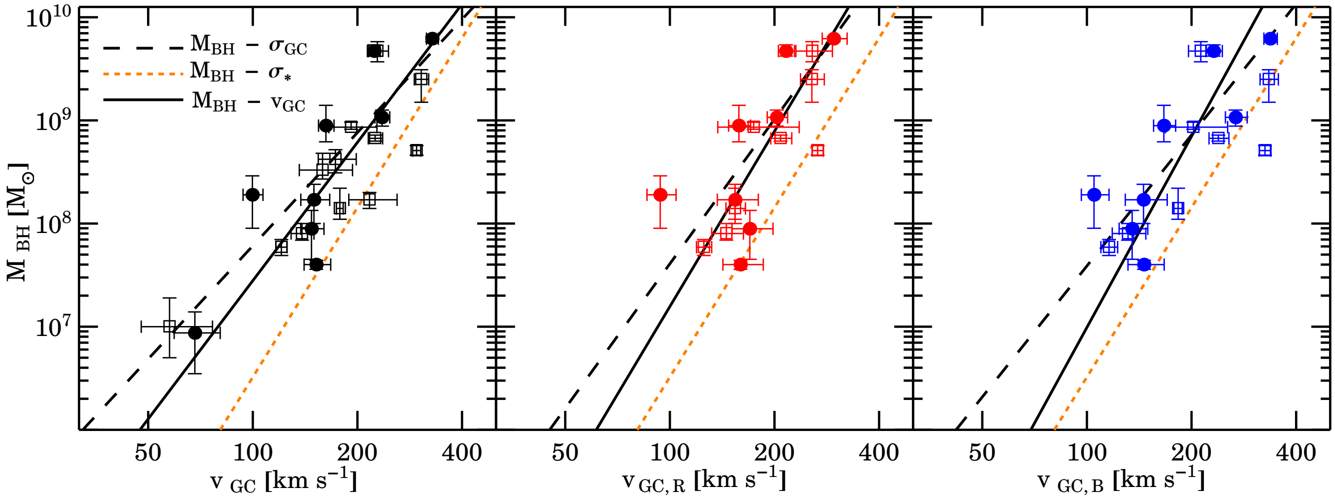

Figure 2. Black hole mass as a function of rotation-included GC system velocity dispersion. Left, central and right panels show the $M_{\rm BH} - v_{\rm GC}$ relation for all, red and blue GCs respectively. Data from the literature and from the SLUGGS survey are shown as open squares and filled points respectively. The black solid line is the best fit to the $M_{\rm BH} - v_{\rm GC}$ relation. The dashed lines are the best-fit to the $M_{\rm BH} - \sigma_{\rm GC}$ relations (whose datapoints are not plotted here for clarity). The slope and the intercept of the best-fit lines are the average between the values from the forward and inverse regression (see Table 1). The dotted-orange line is the stellar $M_{\rm BH} - \sigma_*$ relation from the average between the forward and the inverse regression from Graham et al. (2011): $\alpha = 8.14 \pm 0.05$ and $\beta = 5.54 \pm 0.40$.

		Forward regression				Inverse regression			
Sample	N	α	β	ϵ [dex]	Δ	$\alpha = -\alpha_{\rm inv}/\beta_{\rm inv}$	$\beta = 1/\beta_{\rm inv}$	$\epsilon = \epsilon_{\rm inv}/\beta_{\rm inv}$ [dex]	Δ
$M_{\rm BH} - \sigma_{\rm GC}$	21	$8.76^{+0.11}_{-0.11}$	$3.22^{+0.48}_{-0.33}$	$0.42^{+0.06}_{-0.09}$	0.41	$8.86^{+0.13}_{-0.12}$	$4.35^{+1.02}_{-0.61}$	$0.48^{+0.07}_{-0.11}$	0.51
$(M_{\rm BH} > 10^7 M_\odot) - v_{\rm GC}$	19	$8.75^{+0.11}_{-0.11}$	$3.85^{+0.93}_{-0.76}$	$0.43^{+0.10}_{-0.06}$	0.44	$8.80^{+0.14}_{-0.13}$	$6.18^{+1.37}_{-0.97}$	$0.54^{+0.08}_{-0.13}$	0.57
$M_{\rm BH} - v_{\rm GC}$	21	$8.75^{+0.11}_{-0.10}$	$3.74^{+0.59}_{-0.46}$	$0.40^{+0.09}_{-0.06}$	0.42	$8.83^{+0.12}_{-0.12}$	$5.16^{+0.91}_{-0.62}$	$0.47^{+0.07}_{-0.12}$	0.52
$(M_{\rm BH} > 10^7 M_\odot) - \sigma_{\rm GC}$	19	$8.83^{+0.12}_{-0.10}$	$3.59^{+0.84}_{-0.66}$	$0.41^{+0.10}_{-0.06}$	0.42	$8.93^{+0.15}_{-0.13}$	$5.63^{+1.18}_{-0.88}$	$0.52^{+0.07}_{-0.12}$	0.53
$M_{\rm BH} - \sigma_*$	21	$8.46^{+0.07}_{-0.10}$	$4.44^{+0.74}_{-0.50}$	$0.35^{+0.08}_{-0.05}$	0.37	$8.44^{+0.08}_{-0.11}$	$5.48^{+1.08}_{-0.68}$	$0.39^{+0.06}_{-0.09}$	0.42
$M_{\rm BH} - \sigma_{\rm GC,B}$	16	$8.75^{+0.14}_{-0.12}$	$3.45^{+0.63}_{-0.63}$	$0.47^{+0.07}_{-0.12}$	0.46	$8.82^{+0.19}_{-0.16}$	$5.37^{+1.14}_{-0.86}$	$0.58^{+0.09}_{-0.15}$	0.59
$M_{\rm BH} - v_{\rm GC,B}$	16	$8.73^{+0.13}_{-0.11}$	$3.50^{+0.72}_{-0.68}$	$0.45^{+0.07}_{-0.12}$	0.45	$8.75^{+0.16}_{-0.15}$	$5.53^{+1.17}_{-0.87}$	$0.56^{+0.09}_{-0.16}$	0.57
$M_{\rm BH} - \sigma_{\rm GC,R}$	16	$8.87^{+0.14}_{-0.12}$	$3.77^{+0.93}_{-0.64}$	$0.47^{+0.07}_{-0.13}$	0.47	$9.02^{+0.14}_{-0.16}$	$5.98^{+1.51}_{-1.07}$	$0.60^{+0.10}_{-0.16}$	0.60
$M_{\rm BH} - v_{\rm GC,R}$	16	$8.85^{+0.12}_{-0.12}$	$4.50^{+1.26}_{-0.97}$	$0.44^{+0.07}_{-0.13}$	0.47	$8.93^{+0.15}_{-0.14}$	$6.77^{+1.46}_{-1.11}$	$0.54^{+0.09}_{-0.16}$	0.59

Table 1. Solutions to $\log(M_{\rm BH}/M_\odot) = \alpha + \beta \log(\sigma_{\rm GC}/200\,{\rm km\ s}^{-1})$ for different GC subsets. Shown are the sample size N, the intercept α, the slope β, the intrinsic scatter ϵ and the total rms scatter Δ in the $\log M_{\rm BH}$ direction for both the forward (minimise $\log M_{\rm BH}$ residual) and for the inverse regression (minimise $\log \sigma$ residual).

We will refer to the rotation-subtracted velocity dispersion of the *red*, *blue* and *all* GCs as $\sigma_{\rm GC,R}$, $\sigma_{\rm GC,B}$, $\sigma_{\rm GC}$ respectively.

The second quantity, $v_{\rm GC}$, does not assume a Gaussian velocity distribution and it represents the azimuthally averaged second-order velocity moment which includes rotation:

$$v^2_{\rm GC} = \frac{1}{N}\sum_{i=1}^{N}(v_{\rm i} - v_{\rm sys})^2 - (\Delta v_{\rm i})^2. \qquad (2)$$

where N is the sample size and $\Delta v_{\rm i}$ is the uncertainty on the radial velocity v_i of the i$^{\rm th}$ globular cluster. The uncertainty on $v_{\rm GC}$ is estimated through the formula from Danese et al. (1980). We will refer to $v_{\rm GC}$ of the *red*, *blue* and *all* GCs as $v_{\rm GC,R}$, $v_{\rm GC,B}$, $v_{\rm GC}$ respectively.

The difference between $\sigma_{\rm GC}$ and $v_{\rm GC}$ is that the former represents the rotation-subtracted velocity dispersion whereas the latter also includes the rotation of the spheroid and it is a better reflection of specific kinetic energy. A comparison between $\sigma_{\rm GC}$ and $v_{\rm GC}$ is given in Figure 1 for our galaxy sample without any GC subpopulation split. The two quantities are consistent with each other when the rotation component is negligible, as seen for several systems.

We perform a "sanity check" on all literature data. We prune GCs deviating more than 3σ from the local GC velocity distribution. We also clip outliers with unreasonably large uncertainty (usually > 100 km s^{-1}) and then we recalculate the respective $\sigma_{\rm GC}$ and $v_{\rm GC}$ to avoid methodology biases.

3.2 The $M_{\rm BH} - \sigma_{\rm GC}$ and $M_{\rm BH} - v_{\rm GC}$ relations for GC systems

Here we describe how we characterize the $M_{\rm BH} - \sigma_{\rm GC}$ relation. The procedure is identical for the $M_{\rm BH} - v_{\rm GC}$ relation.

In logarithmic space, $M_{\rm BH}$ and $\sigma_{\rm GC}$ appear to be linearly correlated. The relation we want to study is therefore:

$$\log\left(\frac{M_{\rm BH}}{M_\odot}\right) = \alpha + \beta \log\left(\frac{\sigma_{\rm GC}}{200\,{\rm km\ s^{-1}}}\right), \qquad (3)$$

where α and β are the intercept and the slope of the relation. The numerical constant (200 km s^{-1}) is the normalization factor adopted in similar studies of the stellar $M_{\rm BH} - \sigma_*$ relation. We then use the χ^2–minimization technique (Press et al. 1992) as modified by Tremaine et al. (2002). This ensures that the best fit to Equation 3 is not biased in the case of large uncertainties (Park et al. 2012). Our minimization function is, using the notation $y = \alpha + \beta x$:

$$\chi^2(\alpha,\beta) \equiv \sum_{i=1}^{N} \frac{(y_i - \alpha - \beta x_i)^2}{\epsilon_{y,i}^2 + \beta^2 \epsilon_{x,i}^2 + \epsilon^2} \qquad (4)$$

where ϵ_x and ϵ_y are the errors on x and y respectively. These are defined as $\epsilon_x = (\log \sigma_{\rm upper} - \log \sigma_{\rm lower})/2$ and $\epsilon_y = (\log M_{\rm BH,upper} - \log M_{\rm BH,lower})/2$, respectively. The term ϵ is the intrinsic scatter in the y direction in units of dex. ϵ is iteratively adjusted so that the value of $\chi^2/(N-2)$ equals $1 \pm \sqrt{2/N}$. Uncertainties on α and β were obtained by bootstrapping the sample 2000 times and selecting the 68 per cent confidence interval.

This χ^2 estimator does not treat the data symmetrically in the presence of intrinsic scatter. An "inverse" regression (minimizing the $\log \sigma_{\rm GC}$ residuals rather than the $\log M_{\rm BH}$ residuals) can lead to very different slopes. The latter is preferable in the presence of possible Malmquist-type biases (see Graham et al. 2011). Given our ignorance of the physical mechanisms which links black hole mass to velocity dispersion, there is no reason to believe that the forward regression should be favored over the inverse regression. Therefore, we perform both the "forward" and the "inverse" regression by replacing ϵ in Equation 4 with $\beta^2\epsilon^2$ as suggested by Novak et al. (2006).

4 RESULTS

The $M_{\rm BH} - v_{\rm GC}$ (and the $M_{\rm BH} - \sigma_{\rm GC}$) diagrams for our sample are shown in Figure 2, in which the final slope and intercept of the relations are the average between the forward and the inverse fit. The respective best fit parameters are reported in Table 1.

We find that $M_{\rm BH}$ correlates both with $\sigma_{\rm GC}$ and $v_{\rm GC}$ for all GC subsamples. However, we note that the intrinsic scatter of all our GC subsets are at least two times larger than those reported by SC12. We find that this disagreement is driven by the $M_{\rm BH}$ values of five galaxies in the SC12 sample (marked in Table A1 with "a") for which we have updated $M_{\rm BH}$ measurements. In fact, reanalyzing the SC12 sample using our new velocity dispersion values and the $M_{\rm BH}$ values from SC12 (all from Gültekin et al. 2009 and references therein), we always obtain $\epsilon \leqslant 0.31$ dex, which is in agreement with their findings. Conversely, the regression on the SC12 sample using updated $M_{\rm BH}$ values, returns $\epsilon = 0.38$ dex for the full sample and $\epsilon = 0.44$ dex for the blue and red GC subsets. We conclude that the small intrinsic scatter of SC12 is driven by their black hole mass values and not by their GC system velocity dispersion data. This assumes that the latest values of $M_{\rm BH}$ that we adopt here are also more accurate than those which preceded them.

The slope, intercept and intrinsic scatter of the $M_{\rm BH} - v_{\rm GC}$ and the $M_{\rm BH} - \sigma_{\rm GC}$ relations are consistent with each other within the errors. Similarly, the differences found for the blue and red GCs are not statistically significant. We note that the slopes of the $M_{\rm BH} - v_{\rm GC}$ relations are always steeper than the $M_{\rm BH} - \sigma_{\rm GC}$ ones, because $v_{\rm GC} > \sigma_{\rm GC}$ at low masses. Also, the smaller intrinsic scatter with $v_{\rm GC}$ suggests that the GC kinetic energy (rotation plus dispersion) is a better predictor of black hole masses than the rotation-subtracted velocity dispersion.

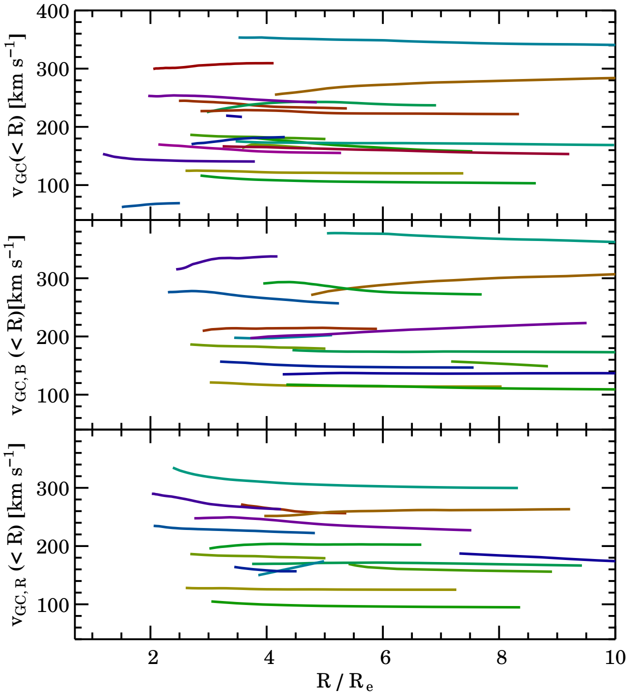

Figure 3. Cumulative root-mean-square velocity dispersion profiles. The plot shows the rotation-included velocity dispersion profiles within a certain radius for all (top panel), blue (central panel) and red GCs (bottom panel). A running mean is used. Different colors represent different galaxies. Most of the profiles are generally flat at all radii.

The intrinsic scatter of the $M_{\rm BH} - v_{\rm GC}$ and $M_{\rm BH} - \sigma_{\rm GC}$ relations are slightly larger than that of the stellar $M_{\rm BH} - \sigma_*$ relation from McConnell & Ma (2012) and Graham & Scott (2012), who both find $\epsilon \sim 0.4$ dex. The best-fit to the stellar $M_{\rm BH} - \sigma_*$ relation computed using our 21 galaxies has an intrinsic scatter of $\epsilon = 0.35^{+0.08}_{-0.05}$ dex in the $\log M_{\rm BH}$ direction, which is also consistent with previous findings.

Lastly, it is noted that the stellar $M_{\rm BH} - \sigma_*$ relation in Figure 2 is shifted towards larger velocity dispersion values with respect to the $M_{\rm BH}-$ (GC system velocity dispersion) relations. This offset is expected because σ_* and the GC system velocity dispersion sample different regions, and maybe different physics, of the galaxy velocity dispersion profile. The stellar velocity dispersion, which probes $(R < R_e)$, is usually larger than the GC system velocity dispersion, which usually probes $R > R_e$. The difference $(\sigma_* - v_{\rm rms,A})$ is found to have a mean of 35 ± 6 km s^{-1} for our 21 galaxies.

4.1 Radial trends

It is interesting to see if the properties of the $M_{\rm BH} - v_{\rm GC}$ or $M_{\rm BH} - \sigma_{\rm GC}$ relation vary when the velocity dispersion is computed within different galactocentric radii.

To do so, we first normalize the galactocentric radii of each GC system to the host galaxy effective radius. We then perform χ^2 tests (Equation 4) with $v_{\rm GC}$ and $\sigma_{\rm GC}$ computed within different radial bins. For the sake of consistency, we adopt effective

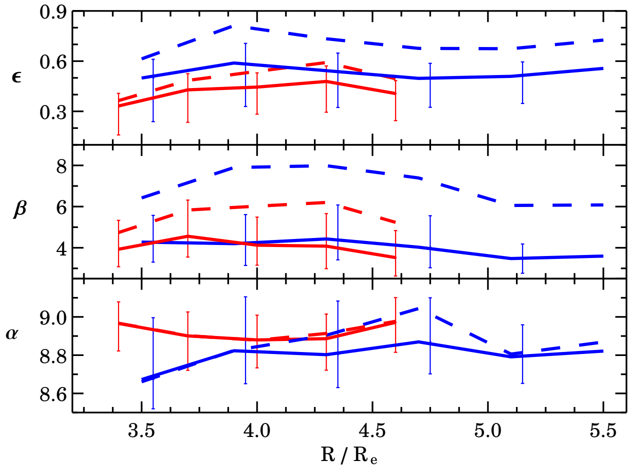

Figure 4. Best-fit $M_{\rm BH}-v_{\rm GC}$ relation within different radial bins. The plot shows how the best-fit α, β and ϵ vary when the $v_{\rm GC}$ is computed within an increasing number of effective radii. Blue and red colours represent the two GC subpopulations. Solid and dashed lines are the results from the forward and the inverse regressions respectively. The horizontal axis is the radius of the outermost GC in a given radial bin. For clarity, only the error bars from the forward regression are shown. None of the radial trends are statistically significant.

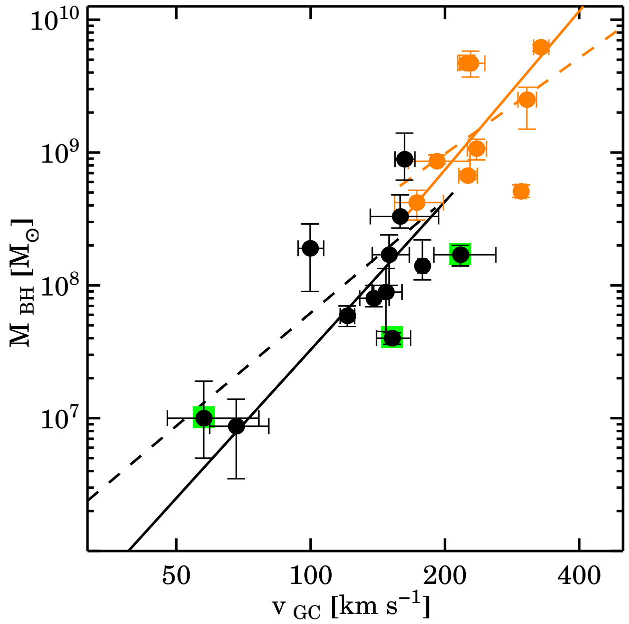

Figure 5. $M_{\rm BH} - v_{\rm GC}$ relation. Orange and black points are galaxies with and without a core in the inner surface brightness profile respectively. The filled and dashed lines are the best fits to core and non-core galaxies when using $v_{\rm GC}$ and $\sigma_{\rm GC}$ respectively. Green boxes mark barred galaxies (NGC 1316, NGC 1023 and NGC 253). The slope of the $M_{\rm BH} - v_{\rm GC}$ relation for core galaxies is consistent within the errors with that of non-core galaxies.

radii values from 2MASS, and we use the transformations from Cappellari et al. (2011) to make them consistent with the values of the RC3 catalogue (de Vaucouleurs 1991).

The cumulative velocity dispersion profiles for our galaxy sample are shown in Figure 3 for all GC subsets. The profiles are generally flat over the radial range probed. It is worth noting that GC dispersion profiles span different radial ranges depending on the galaxy, and we do not extrapolate the dispersion profiles to compensate for this effect. Therefore, the number of GC systems within a given effective radius varies with the radius itself. Demanding a minimum of six GC systems per radial bin, we study the $M_{\rm BH} - v_{\rm GC}$ and the $M_{\rm BH} - \sigma_{\rm GC}$ relations between 3.5 and 5.5 R_e for the blue and the red GC subpopulations.

Results are shown in Figure 4 for the $M_{\rm BH} - v_{\rm GC}$ relation. Each radial bin contains between six to a maximum of eleven GC systems. As expected from the flatness of the velocity dispersion profiles (Figure 3), none of the radial trends seen in Figure 4 are statistically significant. The relations for the blue and the red GC subpopulations are also statistically indistinguishable. There is an hint that the intrinsic scatter for the $M_{\rm BH} - v_{\rm GC,R}$ becomes smaller towards the central regions. This result is biased by the fact that the red GCs tend to be more centrally concentrated than the blue GGs. Given the small number statistics, the best fit to the $M_{\rm BH} - v_{\rm GC}$ relation is independent of radius within which the velocity dispersion is measured, at least for $R > R_e$. The same exercise performed on the rotation-subtracted velocity dispersion $\sigma_{\rm GC}$ leads to a similar result.

A caveat to bear in mind is the way the GC system velocity dispersion is computed. Ideally, one should weight the velocity dispersion for the GC surface density within a certain radius, similarly to what is done for the stellar velocity dispersion σ_* (see Equation 1 in McConnell & Ma 2012). Similarly, the scale radius used in Figure 3 should be the GC system's effective radius and not the host galaxy's effective radius. However, GC surface density profiles are not available for all our galaxies. They are also dependent on variables such as GC selection criteria and imaging field-of-view, which have been carried out differently in the literature.

On the other hand, total GC system size scales with galaxy effective radius (Kartha et al. in prep.) and we see no strong variation of GC system velocity dispersion with radius.

4.2 Cores and bars

The stellar $M_{\rm BH} - \sigma_*$ relation is different for galaxies with or without bars (Graham et al. 2011). It is thought that the orbital structure of the bar may elevate the apparent bulge velocity dispersion (Bureau & Athanassoula 1999), resulting in an offset $M_{\rm BH} - \sigma_*$ relation for barred galaxies with the appropriate bar orientation. On the other hand, the $M_{\rm BH} - \sigma_*$ relation does not differ for non-barred galaxies with or without a 'core' in the inner surface brightness profile (Graham & Scott 2012). An exception may however exist for ultramassive black holes such as those in NGC 3842 and NGC 4489 (McConnell et al. 2011). If these are included in the fit, the $M_{\rm BH} - \sigma_*$ relation for core galaxies is steeper $(\beta \sim 7.0)$ than that for non-core galaxies.

We have tested if the trends seen for 'core' and barred galaxies with stellar data are also present in our $M_{\rm BH} - v_{\rm GC}$ and $M_{\rm BH} - \sigma_{\rm GC}$ relations. To avoid low number statistics issues, we only look at the whole GC population, without any colour split.

Our sample contains only three barred galaxies (NGC 1023, NGC 1316 and NGC 253), preventing any statistical analysis. For the sake of completeness, we note that NGC 1023 and NGC 1316 are indeed offset to higher velocity dispersions relative to the best-fit $M_{\rm BH} - v_{\rm GC}$ relation (Figure 5). However, only NGC 1023 is offset when considering $\sigma_{\rm GC}$. NGC 253 is neither offset from the

$M_{\rm BH}-v_{\rm GC}$ nor the $M_{\rm BH}-\sigma_{\rm GC}$ relation, in agreement with what was found for stellar data.

Regarding 'core' galaxies, our sample contains nine core galaxies and twelve non-core galaxies (see Table A1). The centre of the galaxy NGC 1407 is actually unclassified, but assume this galaxy to have a central core given its mass. We treat NGC 1316 (Fornax A) as a cored galaxy (Faber et al. 1997), but the reader should see the cautionary remarks in Graham & Scott (2012) regarding this galaxy's lack of a bulge/disc decomposition.

The relation between $M_{\rm BH}$ and GC system velocity dispersion for core/non-core galaxies is shown in Figure 5. We remind the reader that the final slope of the $M_{\rm BH}-$ (GC system velocity dispersion) relations is the average between the forward and the inverse regression. Using the uncertainty on the slope and intercept of each regression, we derived a weighted mean to account for the large uncertainties caused by low number statistics. For non-core galaxies, we obtain a slope of $\beta = 3.6 \pm 1.5$ and $\beta = 2.8 \pm 1.5$ for the $M_{\rm BH}-\sigma_{\rm GC}$ and $M_{\rm BH}-v_{\rm GC}$ relations respectively. For core galaxies, the uncertainty on the slope from the inverse regression is larger than the slope itself. This means that the final slope of this relation is driven only by that of the forward regression. In this case, we find $\beta = 2.2 \pm 1.6$ and $\beta = 2.4 \pm 1.6$ for the $M_{\rm BH}-\sigma_{\rm GC}$ and $M_{\rm BH}-v_{\rm GC}$ relations respectively. In conclusion, the $M_{\rm BH}-$ (GC system velocity dispersion) relations for core and non-core galaxies are consistent with each other as found by Graham & Scott (2012) with stellar velocity dispersion data.

Galaxy	Type	$v_{\rm GC}$ [km s^{-1}]	$M_{\rm BH}$ [$M_\odot$]	Ref.
NGC 1380	S0	160^{+23}_{-17}	$2.2^{+1.8}_{-0.9} \times 10^8$	1
NGC 3311	cD	653^{+48}_{-40}	$1.2^{+0.4}_{-0.3} \times 10^{11}$	2
NGC 3923	E4	273^{+42}_{-29}	$2.4^{+2.1}_{-0.9} \times 10^9$	3
NGC 4636	E2	212^{+11}_{-10}	$7.9^{+2.0}_{-1.5} \times 10^8$	4
NGC 4406	E3	295^{+54}_{-36}	$3.4^{+3.8}_{-1.5} \times 10^9$	5
VCC 1261	dE	56^{+18}_{-11}	$2.1^{+5.1}_{-1.3} \times 10^6$	6
VCC 1528	dE	52^{+22}_{-15}	$1.5^{+5.7}_{-1.1} \times 10^6$	7
VCC 1087	dE	41^{+14}_{-10}	$5.2^{+14}_{-3.7} \times 10^5$	8
NGC 1400	S0	137^{+14}_{-11}	$1.1^{+0.6}_{-0.3} \times 10^8$	9
NGC 2768	E6	165^{+13}_{-11}	$2.6^{+1.0}_{-0.6} \times 10^8$	10
NGC 4278	E2	177^{+9}_{-7}	$3.5^{+0.8}_{-0.6} \times 10^8$	11
NGC 4365	E3	248^{+12}_{-10}	$1.6^{+0.3}_{-0.2} \times 10^9$	12
NGC 4494	E1	99^{+14}_{-12}	$2.6^{+2.1}_{-1.1} \times 10^7$	13

Table 2. Black hole mass predictions. Listed from the left to right are: galaxy name, morphological type, GC root-mean-square velocity dispersion, predicted black hole mass from Equation 5 and the GC references. Galaxies below the horizontal line are from the SLUGGS survey. References to GC data are: 1, Puzia et al. (2004); 2, Misgeld et al. (2011); 3, Norris et al. (2012); 4, Lee et al. (2010); 5, Park et al. (2012); 6, 7, Beasley et al. (2009); 8, Beasley et al. (2006); 9,10,11,12, Pota et al. (2013); 13, Foster et al. (2011).

4.3 Predicting $M_{\rm BH}$ in other galaxies

We exploit the best fit $M_{\rm BH}-$ (GC system velocity dispersion) relations found in this work to predict $M_{\rm BH}$ in galaxies without direct black hole mass measurements. We collected a sample of 13 galaxies with GC system kinematic information, listed in Table 2. The first four galaxies were re-analyzed in Pota et al. (2013) with the methods described in §3.1. Similarly, we re-analyzed the GC system kinematics of NGC 4406 (Park et al. 2012) and of three luminous Virgo dwarf ellipticals (dEs) from Beasley et al. (2009) and Beasley et al. (2006). Given that the $M_{\rm BH}-$ (GC system velocity dispersion) relations for the blue and the red GC subpopulations return consistent results, we decided to use the best fit $M_{\rm BH}-v_{\rm GC}$ relation:

$$\log\left(\frac{M_{\rm BH}}{M_\odot}\right) = 8.79 + 4.45 \log\left(\frac{v_{\rm GC}}{200\,{\rm km\,s^{-1}}}\right) \quad (5)$$

where the slope and the intercept of this relation are the average between the forward and the inverse regression from Table 1.

Predicted black hole masses are given in Table 2. Particular emphasis should be given to the three Virgo dEs, whose predicted $M_{\rm BH}$ falls into the range of intermediate mass black holes ($\lesssim 10^6 M_\odot$). All three dEs are known to have a nuclear star cluster (Ferrarese et al. 2006), whose masses are about one order of magnitude larger than our predicted black hole masses, as is expected (Scott & Graham 2013). In fact, the relation between the mass of the nuclear star cluster $M_{\rm NC}$ and stellar velocity dispersion σ_* does not run parallel to the stellar $M_{\rm BH}-\sigma_*$. At fixed $\sigma_* \lesssim 150$ km s^{-1}, Graham & Scott (2012) shows that $M_{\rm NC} > M_{\rm BH}$, which is in agreement with our findings.

It is also worth noting that NGC 3311, the dominant elliptical galaxy of the Hydra Cluster, is at first glance predicted to host an ultramassive black hole candidate with $M_{\rm BH} \sim 10^{11} M_\odot$. However, caveats here are the inclusion of ultra compact dwarfs (UCDs) which make up half of the kinematic sample of this galaxy. UCDs can be kinematically distinct from the underlying GC system (e.g. Strader et al. 2011) and they can bias the velocity dispersion calculation. Another source of contamination might come from intra-cluster UCDs/GCs (Misgeld et al. 2011; Richtler et al. 2011). Excluding the 52 UCDs and looking only at the GC sample, which may still be biased by the cluster potential, we obtain $M_{\rm BH} = 8.4^{+4.7}_{-2.6} \times 10^{10}$. This is still more massive than the most massive SMBH known today (McConnell et al. 2011).

5 DISCUSSION AND CONCLUSIONS

The aim of this paper was to test how well the velocity dispersion of extragalactic globular cluster systems correlates with the mass of supermassive black holes. This was motivated by the work of Sadoun & Colin (2012) who found an intriguingly tight correlation using 12 globular cluster systems.

In this work we have extended this study to a sample of 21 GC systems and we have used the latest compilation of SMBH masses. We confirm that the velocity dispersion of GC systems correlates with SMBH mass. However, this correlation is less significant than that inferred by Sadoun & Colin (2012). The tight correlation found by these authors was driven by old, and possibly less accurate, black hole mass values. We observe an rms scatter in excess of 0.4 dex in the $\log M_{\rm BH}$ direction.

We looked at the correlation between $M_{\rm BH}$ and the velocity dispersion of the blue and the red GC subpopulations separately. Different scatters are expected if blue and red GC systems trace the kinematics of the halo and the bulge of the host galaxy respectively. In the case of a stronger correlation with red GCs, this would suggest that SMBHs grew along with the stellar bulge. Conversely, a stronger correlation with blue GCs would suggest that SMBHs formation is more closely related with the halo. Our current results cannot discriminate between these two scenarios. In general, we find no significant difference between the $M_{\rm BH}-$ (GC system velocity dispersion) relation for the blue and the red GCs. This can be due to some factors discussed below.

Ideally, one should analyze the bluer and the redder GCs for each GC system to avoid contamination in proximity to the blue/red dividing colour. This can make a difference in the final value of the GC system velocity dispersion (Pota et al. 2013). At the same time, this would decrease the number statistics for most of the galaxies. Also, uneven GC spatial sampling can affect the final kinematic outcome, as seen for NGC 4636 in Schuberth et al. (2012).

We have looked at the $M_{\rm BH}-$ (GC system velocity dispersion) relation computing the GC system velocity dispersion within different galactocentric radii, obtaining no significant trends with radius. Collectively, this suggests either that the $M_{\rm BH}-$ (GC system velocity dispersion) relation is secondary, or that a larger galaxy sample will be needed to discriminate which of the GC subpopulation trends is the stronger.

We have looked for possible trends in the $M_{\rm BH}-$ (GC system velocity dispersion) relation for core/non-core galaxies, finding similar slopes, in agreement with stellar velocity dispersion results (Graham & Scott 2012).

The best fit relation between $M_{\rm BH}$ and the rotation-included GC system velocity dispersion has been used to predict black hole masses in 13 galaxies. This implies that NGC 3311 contains an ultramassive black hole with $M_{\rm BH} \sim 10^{11} M_{\odot}$.

ACKNOWLEDGEMENTS

We thank the anonymous referee for the constructive feedback. Some of the data presented herein were obtained at the W. M. Keck Observatory, operated as a scientific partnership among the California Institute of Technology, the University of California and the National Aeronautics and Space Administration, and made possible by the generous financial support of the W. M. Keck Foundation. The authors wish to recognize and acknowledge the very significant cultural role and reverence that the summit of Mauna Kea has always had within the indigenous Hawaiian community. The analysis pipeline used to reduce the DEIMOS data was developed at UC Berkeley with support from NSF grant AST-0071048. This work is based in part on data collected at Subaru Telescope and obtained from the SMOKA (which is operated by the Astronomy Data Centre, National Astronomical Observatory of Japan), via a Gemini Observatory time exchange. AWG is supported by the Australia Research Council (DP110103509 and FT110100263). This work was supported by NSF grants AST-0909037 and AST-1211995. This research has made use of the NASA/IPAC Extragalactic Database (NED) which is operated by the Jet Propulsion Laboratory, California Institute of Technology, under contract with the National Aeronautics and Space Administration. We acknowledge the usage of the HyperLeda database (http://leda.univ-lyon1.fr).

REFERENCES

Alves-Brito A., Hau G. K. T., Forbes D. A., Spitler L. R., Strader J., Brodie J. P., Rhode K. L., 2011, MNRAS, 417, 1823

Arnold J. A., Romanowsky A. J., Brodie J. P., Chomiuk L., Spitler L. R., Strader J., Benson A. J., Forbes D. A., 2011, ApJ, 736, L26

Ashman K. M., Zepf S. E., 1992, ApJ, 384, 50

Beasley M. A., Cenarro A. J., Strader J., Brodie J. P., 2009, AJ, 137, 5146

Beasley M. A., Forbes D. A., Brodie J. P., Kissler-Patig M., 2004, MNRAS, 347, 1150

Beasley M. A., Sharples R. M., 2000, MNRAS, 311, 673

Beasley M. A., Strader J., Brodie J. P., Cenarro A. J., Geha M., 2006, AJ, 131, 814

Bergond G., Zepf S. E., Romanowsky A. J., Sharples R. M., Rhode K. L., 2006, A&A, 448, 155

Brodie J. P., Strader J., 2006, ARA&A, 44, 193

Bureau M., Athanassoula E., 1999, ApJ, 522, 686

Burkert A., Tremaine S., 2010, ApJ, 720, 516

Cappellari M., Emsellem E., Krajnović D., McDermid R. M., Scott N., Verdoes Kleijn G. A., Young L. M., Alatalo K., Bacon R., Blitz L., Bois M., Bournaud F., Bureau M., Davies R. L., 2011, MNRAS, 413, 813

Côté P., 1999, AJ, 118, 406

Côté P., Marzke R. O., West M. J., 1998, ApJ, 501, 554

Côté P., McLaughlin D. E., Cohen J. G., Blakeslee J. P., 2003, ApJ, 591, 850

Côté P., McLaughlin D. E., Hanes D. A., Bridges T. J., Geisler D., Merritt D., Hesser J. E., Harris G. L. H., Lee M. G., 2001, ApJ, 559, 828

Danese L., de Zotti G., di Tullio G., 1980, A&A, 82, 322

de Vaucouleurs G., 1991, Science, 254, 1667

Debattista V. P., Kazantzidis S., van den Bosch F. C., 2013, ArXiv e-prints

Elmegreen B. G., Malhotra S., Rhoads J., 2012, ApJ, 757, 9

Emsellem E., Cappellari M., Krajnović D., Alatalo K., Blitz L., Bois M., Bournaud F., Bureau M., Davies R. L., Davis T. A., de Zeeuw P. T., 2011, MNRAS, 414, 888

Faber S. M., Tremaine S., Ajhar E. A., Byun Y.-I., Dressler A., Gebhardt K., Grillmair C., Kormendy J., Lauer T. R., Richstone D., 1997, AJ, 114, 1771

Ferrarese L., Côté P., Jordán A., Peng E. W., Blakeslee J. P., Piatek S., Mei S., Merritt D., Milosavljević M., Tonry J. L., West M. J., 2006, ApJS, 164, 334

Forbes D. A., Brodie J. P., Grillmair C. J., 1997, AJ, 113, 1652

Forbes D. A., Cortesi A., Pota V., Foster C., Romanowsky A. J., Merrifield M. R., Brodie J. P., Strader J., Coccato L., Napolitano N., 2012, MNRAS, 426, 975

Forbes D. A., Ponman T., O'Sullivan E., 2012, MNRAS, 425, 66

Forte J. C., Faifer F., Geisler D., 2005, MNRAS, 357, 56

Foster C., Spitler L. R., Romanowsky A. J., Forbes D. A., Pota V., Bekki K., Strader J., Proctor R. N., Arnold J. A., Brodie J. P., 2011, MNRAS, 415, 3393

Goudfrooij P., Mack J., Kissler-Patig M., Meylan G., Minniti D., 2001, MNRAS, 322, 643

Graham A. W., 2008, ApJ, 680, 143

Graham A. W., Onken C. A., Athanassoula E., Combes F., 2011, MNRAS, 412, 2211

Graham A. W., Scott N., 2012, ArXiv e-prints

Gültekin K., Cackett E. M., Miller J. M., Di Matteo T., Markoff S., Richstone D. O., 2009, ApJ, 706, 404

Gültekin K., Richstone D. O., Gebhardt K., Lauer T. R., Tremaine S., Aller M. C., Bender R., Dressler A., Faber S. M., Filippenko A. V., Green R., Ho L. C., Kormendy J., Magorrian J., Pinkney J., Siopis C., 2009, ApJ, 698, 198

Harris G. L. H., Harris W. E., 2011, MNRAS, 410, 2347

Hopkins P. F., Hernquist L., Cox T. J., Robertson B., Krause E., 2007, ApJ, 669, 67

Hu J., 2008, MNRAS, 386, 2242

Hwang H. S., Lee M. G., Park H. S., Kim S. C., Park J.-H., Sohn Y.-J., Lee S.-G., Rey S.-C., Lee Y.-W., Kim H.-I., 2008, ApJ,

674, 869
Jahnke K., Macciò A. V., 2011, ApJ, 734, 92
Krajnović D., Cappellari M., de Zeeuw P. T., Copin Y., 2006, MNRAS, 366, 787
Kruijssen J. M. D., Pelupessy F. I., Lamers H. J. G. L. M., Portegies Zwart S. F., Bastian N., Icke V., 2012, MNRAS, 421, 1927
Lee M. G., Hwang H. S., Kim S. C., Park H. S., Geisler D., Sarajedini A., Harris W. E., 2008, ApJ, 674, 886
Lee M. G., Park H. S., Hwang H. S., Arimoto N., Tamura N., Onodera M., 2010, ApJ, 709, 1083
Mayer L., Kazantzidis S., Escala A., Callegari S., 2010, Nature, 466, 1082
McConnell N. J., Ma C.-P., 2012, ArXiv e-prints
McConnell N. J., Ma C.-P., Gebhardt K., Wright S. A., Murphy J. D., Lauer T. R., Graham J. R., Richstone D. O., 2011, Nature, 480, 215
Mei S., Blakeslee J. P., Côté P., Tonry J. L., West M. J., Ferrarese L., Jordán A., Peng E. W., Anthony A., Merritt D., 2007, ApJ, 655, 144
Misgeld I., Mieske S., Hilker M., Richtler T., Georgiev I. Y., Schuberth Y., 2011, A&A, 531, A4
Moore B., Diemand J., Madau P., Zemp M., Stadel J., 2006, MNRAS, 368, 563
Nantais J. B., Huchra J. P., 2010, AJ, 139, 2620
Norris M. A., Gebhardt K., Sharples R. M., Faifer F. R., Bridges T., Forbes D. A., Forte J. C., Zepf S. E., Beasley M. A., Hanes D. A., Proctor R., Kannappan S. J., 2012, MNRAS, 421, 1485
Novak G. S., Cox T. J., Primack J. R., Jonsson P., Dekel A., 2006, ApJ, 646, L9
Oliva E., Origlia L., Kotilainen J. K., Moorwood A. F. M., 1995, A&A, 301, 55
Olsen K. A. G., Miller B. W., Suntzeff N. B., Schommer R. A., Bright J., 2004, AJ, 127, 2674
Omukai K., Schneider R., Haiman Z., 2008, ApJ, 686, 801
Park D., Kelly B. C., Woo J.-H., Treu T., 2012, ArXiv e-prints
Park H. S., Lee M. G., Hwang H. S., 2012, ApJ, 757, 184
Pierce M., Beasley M. A., Forbes D. A., Bridges T., Gebhardt K., Faifer F. R., Forte J. C., Zepf S. E., Sharples R., Hanes D. A., Proctor R., 2006, MNRAS, 366, 1253
Pota V., Forbes D. A., Romanowsky A. J., Brodie J. P., Spitler L. R., Strader J., Foster C., Arnold J. A., Benson A., Blom C., Hargis J. R., Rhode K. L., Usher C., 2013, MNRAS, 428, 389
Press W. H., Teukolsky S. A., Vetterling W. T., Flannery B. P., 1992, Numerical recipes in C. The art of scientific computing
Proctor R. N., Forbes D. A., Romanowsky A. J., Brodie J. P., Strader J., Spolaor M., Mendel J. T., Spitler L., 2009, MNRAS, 398, 91
Puzia T. H., Kissler-Patig M., Thomas D., Maraston C., Saglia R. P., Bender R., Richtler T., Goudfrooij P., Hempel M., 2004, A&A, 415, 123
Rhode K. L., 2012, AJ, 144, 154
Richtler T., Salinas R., Misgeld I., Hilker M., Hau G. K. T., Romanowsky A. J., Schuberth Y., Spolaor M., 2011, A&A, 531, A119
Sadoun R., Colin J., 2012, MNRAS, 426, L51
Schuberth Y., Richtler T., Hilker M., Dirsch B., Bassino L. P., Romanowsky A. J., Infante L., 2010, A&A, 513, A52
Schuberth Y., Richtler T., Hilker M., Salinas R., Dirsch B., Larsen S. S., 2012, A&A, 544, A115
Scott N., Graham A. W., 2013, ApJ, 763, 76
Shapiro K. L., Genzel R., Förster Schreiber N. M., 2010, MNRAS, 403, L36
Snyder G. F., Hopkins P. F., Hernquist L., 2011, ApJ, 728, L24
Spitler L. R., Romanowsky A. J., Diemand J., Strader J., Forbes D. A., Moore B., Brodie J. P., 2012, MNRAS, 423, 2177
Strader J., Romanowsky A. J., Brodie J. P., Spitler L. R., Beasley M. A., Arnold J. A., Tamura N., Sharples R. M., Arimoto N., 2011, ApJS, 197, 33
Tonry J. L., Dressler A., Blakeslee J. P., Ajhar E. A., Fletcher A. B., Luppino G. A., Metzger M. R., Moore C. B., 2001, ApJ, 546, 681
Tremaine S., Gebhardt K., Bender R., Bower G., Dressler A., Faber S. M., Filippenko A. V., Green R., Grillmair C., Ho L. C., Kormendy J., Lauer T. R., Magorrian J., Pinkney J., Richstone D., 2002, ApJ, 574, 740
Woodley K. A., Gómez M., Harris W. E., Geisler D., Harris G. L. H., 2010, AJ, 139, 1871

APPENDIX A: DATA TABLE

Galaxy [NGC] (1)	Type (2)	D [Mpc] (3)	$M_{\rm BH}$ [$10^8 M_\odot$] (4)	σ_* [km s^{-1}] (5)	Core (6)	σ_A [km s^{-1}] (7)	σ_B [km s^{-1}] (8)	σ_R [km s^{-1} (9)	$v_{\rm GC}$ [km s^{-1}] (10)	$v_{\rm GC,B}$ [km s^{-1}] (11)	$v_{\rm GC,R}$ [km s^{-1}] (12)	Ref. (13)
0224	Sb	0.73	$1.4^{+0.8}_{-0.3}$	160 ± 8	n	134^{+5}_{-5}	129^{+8}_{-6}	121^{+9}_{-10}	178^{+4}_{-4}	183^{+5}_{-5}	154^{+11}_{-9}	1
0253	SBc	3.5	$0.1^{+0.05}_{-0.1}$	109 ± 10	n	37^{+6}_{-7}	–	–	58^{+16}_{-13}	–	–	2
0524	S0	24.2	$8.6^{+1.0}_{-0.4}$	235 ± 10	y	175^{+15}_{-15}	167^{+23}_{-27}	164^{+27}_{-33}	192^{+36}_{-26}	202^{+52}_{-34}	174^{+61}_{-37}	3
1316	SB0	21.0	$1.7^{+0.3}_{-0.3}$	226 ± 11	y	168^{+38}_{-41}	–	–	217^{+43}_{-28}	–	–	4
1399	E1	19.4	$4.7^{+0.6}_{-0.6}$	296 ± 15	y	293^{+7}_{-8}	321^{+12}_{-12}	269^{+9}_{-10}	296^{+8}_{-8}	325^{+13}_{-12}	266^{+10}_{-9}	5
3031	Sab	4.1	$0.9^{+0.20}_{-0.11}$	143 ± 7	n	120^{+8}_{-9}	124^{+13}_{-13}	99^{+8}_{-8}	139^{+11}_{-10}	131^{+16}_{-13}	145^{+17}_{-13}	6
3379$^{\rm a}$	E1	10.7	$4.2^{+1.0}_{-1.1}$	206 ± 10	y	184^{+15}_{-14}	–	–	173^{+26}_{-19}	–	–	7/8
3585	S0	20.6	$3.3^{+1.5}_{-0.6}$	213 ± 10	n	158^{+20}_{-22}	–	–	159^{+35}_{-23}	–	–	9
4472$^{\rm a}$	E2	16.7	25^{+6}_{-1}	315 ± 16	y	303^{+15}_{-13}	333^{+19}_{-20}	261^{+18}_{-18}	305^{+15}_{-14}	334^{+22}_{-19}	256^{+22}_{-19}	10
4594$^{\rm a}$	Sa	10.0	$6.7^{+0.5}_{-0.4}$	230 ± 12	y	229^{+10}_{-10}	238^{+13}_{-14}	208^{+13}_{-13}	225^{+11}_{-10}	239^{+17}_{-14}	208^{+16}_{-13}	11
4649$^{\rm a}$	E2	16.5	47^{+11}_{-10}	335 ± 17	y	206^{+13}_{-13}	194^{+14}_{-16}	228^{+28}_{-28}	228^{+17}_{-15}	213^{+21}_{-17}	257^{+37}_{-26}	12
5128$^{\rm a}$	S0	4.1	$0.59^{+0.11}_{-0.10}$	150 ± 7	n	121^{+4}_{-4}	118^{+5}_{-5}	123^{+6}_{-6}	121^{+5}_{-4}	116^{+7}_{-6}	125^{+7}_{-6}	13
0821$^{\rm a}$	E6	23.4	$1.7^{+0.7}_{-0.7}$	209 ± 10	n	151^{+13}_{-13}	129^{+19}_{-20}	162^{+20}_{-19}	150^{+17}_{-12}	145^{+25}_{-17}	154^{+26}_{-17}	14
1023	SB0	10.5	$0.4^{+0.04}_{-0.04}$	204 ± 10	n	141^{+10}_{-10}	139^{+15}_{-16}	139^{+16}_{-18}	152^{+15}_{-12}	146^{+21}_{-15}	160^{+26}_{-18}	18
1407	E0	29.0	47^{+7}_{-5}	274 ± 14	y	222^{+8}_{-8}	231^{+11}_{-11}	210^{+11}_{-10}	223^{+9}_{-8}	231^{+13}_{-11}	215^{+12}_{-10}	14
3115	S0	9.5	$8.9^{+5.1}_{-2.7}$	230 ± 11	n	153^{+7}_{-7}	152^{+9}_{-8}	150^{+10}_{-10}	162^{+9}_{-8}	166^{+13}_{-11}	158^{+13}_{-10}	15
3377$^{\rm a}$	E5	11.0	$1.9^{+1.0}_{-1.0}$	145 ± 7	n	91^{+5}_{-6}	99^{+7}_{-7}	78^{+8}_{-8}	100^{+7}_{-6}	105^{+11}_{-8}	94^{+10}_{-8}	14
4473$^{\rm a}$	E5	15.2	$0.89^{+0.45}_{-0.44}$	190 ± 9	n	147^{+9}_{-9}	134^{+11}_{-11}	162^{+14}_{-16}	148^{+13}_{-10}	135^{+15}_{-11}	170^{+28}_{-19}	16
4486$^{\rm a}$	E1	16.7	62^{+3}_{-4}	334 ± 10	y	327^{+12}_{-10}	336^{+16}_{-17}	293^{+27}_{-25}	328^{+14}_{-12}	337^{+16}_{-14}	296^{+28}_{-22}	17
5846	E0	24.2	$10.7^{+1.9}_{-1.9}$	237 ± 10	y	235^{+17}_{-18}	269^{+17}_{-18}	201^{+13}_{-13}	235^{+12}_{-11}	268^{+21}_{-17}	203^{+15}_{-12}	14
7457$^{\rm a}$	S0	12.2	$0.087^{+0.052}_{-0.052}$	67 ± 3	n	40^{+8}_{-9}	–	–	68^{+12}_{-9}	–	–	14

Table A1. Galaxy sample. Galaxy NGC names (1) and Hubble types (2) are from NED database. Galaxy distances (3), SMBH masses (4) and stellar velocity dispersions (5) are from McConnell & Ma (2012) and references therein. If not in McConnell & Ma (2012): distances were obtained by subtracting 0.06 mag (Mei et al. 2007) to the distance modulus from Tonry et al. (2001); central stellar velocity dispersions are weighted values from HyperLeda; $M_{\rm BH}$ are from Oliva et al. (1995) and Hu (2008) for NGC 253 and NGC 5846 respectively. (6) is the presence of a core in the galaxy inner surface brightness profile. Column (7), (8) and (9) are the rotation-subtracted velocity dispersion for all, blue and red GCs respectively. Column (10), (11) and (12) are the root-mean square velocity for all, blue and red GCs respectively. GC references (13) : 1, Lee et al. (2008); 2, Olsen et al. (2004); 3, Beasley et al. (2004); 4, Goudfrooij et al. (2001); 5, Schuberth et al. (2010); 6, Nantais & Huchra (2010); 7, (Pierce et al. 2006); 8, (Bergond et al. 2006); 9, Puzia et al. (2004); 10, Côté et al. (2003); 11, Alves-Brito et al. (2011); 12, Hwang et al. (2008); 13, Woodley et al. (2010); 14, Pota et al. (2013); 15, Arnold et al. (2011); 16, Foster et al. (in prep.); 17, Strader et al. (2011); 18, Pota et al. in prep. GC system velocity dispersion values for NGC 224 are from Lee et al. (2008). Galaxies with updated $M_{\rm BH}$ measurements after Gültekin et al. (2009) are marked with (a).